



The integration of low temperature supercritical water gasification with continuous *in situ* nano-catalyst synthesis for hydrogen generation from biomass wastewater

Chai Siah Lee^{a,b}, Alex V. Conradie^b, Edward Lester^{a,*}

^a Advanced Materials Research Group, Faculty of Engineering, University of Nottingham, Nottingham NG7 2RD, United Kingdom

^b Sustainable Process Technologies Research Group, Faculty of Engineering, University of Nottingham, Nottingham NG7 2RD, United Kingdom

ARTICLE INFO

Keywords:

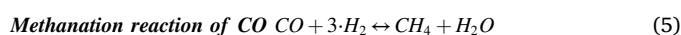
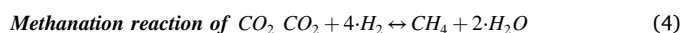
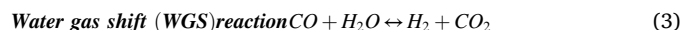
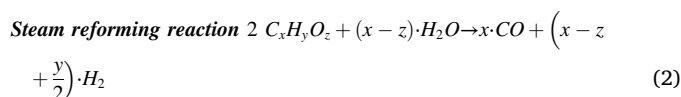
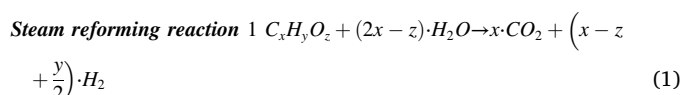
Supercritical water gasification
Biomass wastewater
Partial oxidation
Metal oxide nano-catalyst
Continuous hydrothermal synthesis
Hydrogen

ABSTRACT

A continuous hydrothermal process is demonstrated, for the first time, that can operate at low gasification temperature (430 °C) and residence time (20 s) by combining supercritical water gasification (SCWG) and partial oxidation with *in situ* synthesis of virgin metal oxide nano-catalyst. Using olive wastewater as the feedstock, this gasification study experimentally investigated the impact of multiple variables: (1) COD feed concentration, (2) the *in situ* synthesis of different metal oxide nano-catalysts, (3) the partial oxidation coefficient (η) and (4) the nano-catalyst precursor solution concentration. The optimum conditions for the generation of hydrogen and methane from olive wastewater were a feed COD of 38.6 g/L, $\eta = 0.8$, and 60 mM precursor concentration for the *in situ* synthesis of Fe₂O₃ nano-catalyst. These optimised conditions were further investigated using spent lees and stillage. The efficiency of hydrogen and methane yields and COD reduction were in the order of stillage > spent lees > olive wastewater. The highest hydrogen molar selectivity, hydrogen and methane yields at 18.8 %, 17 and 11.4 mol/(kg biomass) respectively were obtained with stillage feedstock. Gasification, COD and TOC reduction efficiencies were 68.8–71.7 %, 72.6–76.5 % and 53.9–55.7 % respectively, with this process. Importantly, this novel gasification approach prevents any performance drop or catalyst deactivation during continuous operation. This study exemplifies that the co-generation of catalyst during SCWG is a promising and economically feasible direction for large-scale continuous generation of hydrogen and methane from different types of biomass wastewater at < 450 °C, whilst lowering its COD and TOC. (249 words)

1. Introduction

Supercritical water gasification (SCWG) has previously been identified as a suitable and environmentally friendly route for efficient hydrothermal conversion of wet biomass waste, particularly biomass wastewater where hydrogen and methane generation can be achieved simultaneously with wastewater treatment, using supercritical water as a solvent-free reaction medium [1]. Biomass wastewater is a waste output from many manufacturing processes such as from the distillery and dairy sectors and is therefore generally available all year round at a low or negative cost. As such, biomass wastewater can be seen as a renewable energy source with significant potential for hydrogen and methane generation. The main thermochemical SCWG reactions are listed below.



Several wastewater feedstocks have been tested in batch SCWG for hydrogen generation: including landfill leachate [2], rice liquor stillage

* Corresponding author.

E-mail address: Edward.Lester@Nottingham.ac.uk (E. Lester).

<https://doi.org/10.1016/j.cej.2022.140845>

Received 27 July 2022; Received in revised form 24 November 2022; Accepted 5 December 2022

Available online 9 December 2022

1385-8947/© 2022 The Authors. Published by Elsevier B.V. This is an open access article under the CC BY license (<http://creativecommons.org/licenses/by/4.0/>).

[3], black liquor [4,5], wine distillery wastewater [6], sewage sludge [7], the effluent of food waste treatment [8], and olive wastewater [9]. Comparatively, there are fewer continuous flow SCWG studies using wastewater from sewage sludge [10,11], chicken manure [12], poultry manure [13], olive [14–16] and black liquor [17,18]. In these SCWG studies, the principal focus was on hydrogen and methane generation from the wastewater feedstock, with limited consideration of wastewater treatment in terms of COD (chemical oxygen demand) and TOC (total organic carbon) reduction efficiencies.

Complementing these batch and continuous studies, a few studies have investigated the impact of partial oxidation on hydrogen and methane production, by adding an oxidant into the SCWG processing. The wastewater feedstock in these studies includes sewage sludge [19,20], cabbage slurry [21], petrochemical wastewater [22] and hog manure [23] in batch mode; and cutting oil wastewater and vinasses [24] and olive wastewater [25] in continuous flow mode. Most of these studies reported that the application of partial oxidation to the SCWG process not only enhanced the gas yields, but also improved the wastewater treatment efficiency in terms of COD and TOC reduction efficiencies.

Most of the reported continuous flow SCWG processes using wastewater feedstock utilised either a homogeneous catalyst (e.g., NaOH and K_2CO_3) [10,11,24] or a heterogeneous catalyst (e.g., activated carbon, Ru/ Al_2O_3 and Ni/ Al_2O_3) [12–14] in the process, thereby kinetically promoting greater hydrogen yields at operating temperatures below 600 °C. Temperatures above 600 °C are typically reported in the absence of catalysts [26]. Homogeneous catalysts require the continuous addition of fresh catalyst and separation of the catalyst from the reactor effluent can be costly and impractical [27]. Without separation, the environmental consequence may negate the benefit of COD reduction. Consequently, for continuous operation, heterogeneous catalysts are typically packed into the reactor before operation and used throughout the run. However, rapid catalyst deactivation is commonly attributed to charring and sintering, often within minute timescales and this caused a decrease in gasification performance during continuous operation [28–30].

This paper investigates the co-generation of nano-catalyst and gases harbouring reducing power (hydrogen and methane), thereby avoiding the challenges associated with catalyst deactivation, homogenous catalyst separation and/or the need for high operating temperatures. Operating temperatures ~400 °C were found to be possible by combining the SCWG process and partial oxidation with *in situ* synthesis of metal oxide heterogeneous nano-catalyst, via a continuous hydrothermal synthesis process (CHS). CHS is an emerging technology which takes advantage of the tuneable chemical and physical properties of superheated water to produce nano-catalysts via rapid nucleation and growth [31]. The suspended nano-catalyst promotes the kinetics towards generating hydrogen-rich syngas at a low operating temperature, whilst simultaneously reducing the COD and TOC of the wastewater. The co-generation of catalyst and gas product thus avoids the performance drop associated with catalyst deactivation of a fixed bed, and a fraction of the nano-catalyst can be recovered and sold as a secondary product.

Using a range of wastewater feedstocks, this study exemplified the co-generation strategy by (1) screening for a suitable metal oxide nano-catalyst, (2) evaluating the efficacy of partial oxidation and (3) assessing the contribution of nano-catalyst precursor concentration on hydrogen and methane production. Thereby, this study demonstrates that a continuous catalytic SCWG process can be realised at ~400 °C, underpinning lower CAPEX and OPEX than a non-catalytic SCWG process at 600 °C [26,32].

2. Material and methods

Exemplifying the co-generation strategy; firstly, the SCWG-CHS process screened different types of metal oxide nano-catalysts

($AlOOH$, CeO_2 and Fe_2O_3) using a non-catalytic SCWG process as control. This nano-catalyst screen was undertaken at 430 °C and two different feedstock concentrations using olive wastewater as feedstock. The nano-catalysts were recovered and characterised for composition, morphology, and particle size. Secondly, the best performing metal oxide nano-catalyst, i.e., cost-effective Fe_2O_3 , was used at a specific feedstock concentration to investigate the effect of hydrogen peroxide (H_2O_2) as a partial oxidant. Thirdly, the impact of the Fe_2O_3 nano-catalyst precursor concentration on H_2 & CH_4 production and COD reduction was investigated. Finally, the optimised process conditions were used with other wastewater feedstocks available at appreciable scale, i.e. spent lees and stillage, and the results were compared with previously reported literature. The efficiency of this co-generation process in maintaining the gasification performance was established by monitoring the gas yields during 40 min of continuous operation. The studied variables were evaluated based on the gas yields (H_2 , CH_4 , CO and CO_2), hydrogen selectivity, gasification efficiency, COD and TOC reduction efficiencies.

2.1. Materials

Hydrogen peroxide [H_2O_2] (30 % w/v) was purchased from Fisher. Iron(III) nitrate nonahydrate [$Fe(NO_3)_3 \cdot 9H_2O$], aluminium nitrate nonahydrate [$Al(NO_3)_3 \cdot 9H_2O$] and cerium(III) nitrate hexahydrate [$Ce(NO_3)_3 \cdot 6H_2O$] were purchased from Sigma-Aldrich and were used as the precursor metal salts to form iron(III) oxide, aluminium hydroxide oxide and cerium(IV) oxide nano-catalysts respectively. Deionised water was used to make feed solutions at different molar concentrations.

2.2. Source of biomass wastewater

Olive wastewater was obtained from an olive processing mill in Spain. Spent lees, i.e., the wastewater generated after the distillation stage in the production of gins using grain neutral spirit as the base, was obtained from Warner's Distillery Ltd, UK. Stillage, classified as concentrated wheat distillers soluble, was obtained from Sedamyl UK. Stillage is a by-product from potable alcohol production based on wheat starch and is commonly used as animal feed. All the biomass wastewater and SCWG products were stored at ~4 °C until analysis or use.

2.3. Characterisation of biomass wastewaters

All wastewaters were characterised by pH, moisture content, total suspended solids (TSS), total dissolved solids (TDS), chemical oxygen demand (COD) and total organic carbon (TOC). Proximate analysis was utilised to determine volatile matter, fixed carbon and ash content for each wastewater. Ultimate analysis was utilised to determine the carbon (C), hydrogen (H), oxygen (O), nitrogen (N) and sulphur (S) content for each wastewater. For the proximate and ultimate analysis, a certain volume of biomass wastewater was filtered with Whatman 1004–070 (20–25 μm pore size) filter paper and then dried at low temperature (30 °C) in an oven to prevent biodegradation of bioactive compounds until a constant weight was obtained. The dried samples were ground with a mortar and pestle to obtain a dried powder.

2.3.1. pH analysis

The pH of each type of wastewater was measured with a Jenway 3540 pH & conductivity meter. The pH meter was calibrated using pH 4, pH 7 and pH 10 buffer solutions before use.

2.3.2. TSS and TDS analysis

The biomass wastewater was filtered with Whatman 1004–070 (20–25 μm pore size) filter paper. The solid residue that was retained on the filter paper and the filtrate were dried in an oven at 105 °C until a constant weight was obtained for the determination of the TSS and TDS respectively.

2.3.3. COD analysis

The raw and treated biomass wastewater was centrifuged at 4000 rpm for 15 min, followed by filtration using Whatman 1004–070 (20–25 µm pore size) filter paper to remove the suspended solids in the wastewater. The filtrates were diluted to the concentration ranges of 5–60 g/L O₂ for the raw wastewater or 0–1 g/L O₂ for the treated wastewater before the COD analysis. The diluted filtrates were tested for COD using the COD cuvette tests LCK014 and LCI400 (HACH LANGE Ltd, Manchester, UK) following ISO 15705. The test involved oxidising the organic content of liquid samples under acidic conditions for 2 h at 148 °C which produced water, CO₂ and trivalent chromium. The detection of the trivalent chromium was measured at 605 nm using a DR 2800 spectrophotometer.

2.3.4. TOC analysis

The biomass wastewater was centrifuged and filtered using the same procedures as the COD analysis. The diluted filtrates were tested for TOC using the TOC cuvette test LCK 381 (HACH LANGE Ltd, Manchester, UK). The test entails oxidising the total carbon and total inorganic carbon of liquid samples to CO₂ under acidic conditions for 2 h at 100 °C. CO₂ was passed from the digestion cuvette through a membrane and into the indicator cuvette. The degree of the colour change of the indicator was photometrically evaluated at 435 nm using a DR 2800 spectrophotometer. TOC was determined as the difference between the total carbon and total inorganic carbon values.

2.3.5. Proximate analysis

The proximate analysis was conducted with a thermogravimetric analyser (TGA Q500A) following the method developed for characterising biomass materials [33] with slight modification. The dried samples were heated from room temperature to 900 °C in nitrogen (100 mL/min) at a heating rate of 5 °C/min and held for 5 min at 900 °C for volatile matter determination. Afterwards, the gas was changed to air at 100 mL/min and held at 900 °C for 20 min for the quantification of fixed carbon with the final weight representing the ash content.

2.3.6. Ultimate/elemental analysis

The ultimate analysis of biomass wastewaters (CHN and S) was determined using the Leco CHN 628 and 628 S instruments [34]. Approximately 0.15–0.20 g of dried sample was used for each test and repeated five times.

2.4. Catalytic SCWG with *in situ* synthesis of nano-catalyst

All reactions were conducted at a laboratory scale under continuous mode. A simplified scheme of the experimental rig is shown in Fig. S1. Gilson HPLC pumps (Model 305 equipped with a 25 SC pump head) were used for water and biomass wastewater and oxidant delivery. K-type thermocouples were used for monitoring temperature at different locations. All parts, fittings and tubing were made from 316L stainless steel sourced from Swagelok.

The water discharge of the high-pressure pump was preheated through a coiled heater, a tube of 6 m length of 1/4" outer diameter (OD), to the desired supercritical temperature. After the heater, the supercritical water flowed downwards at 10 mL/min into the open-ended, inner tube (1/8" OD) of the reactor's annulus (concentric tube-in-tube) configuration (Fig. S2), heated on the outside using a 1 kW Watlow band heater. Flowing upwards into the outer tube (3/8" OD) of the reactor's annulus configuration, the filtered biomass wastewater solution and the H₂O₂ solution were pressurised and mixed with the supercritical water delivered at the open-ended, inner tube at the base of the reactor. The wastewater and H₂O₂ solutions were fed at room temperature, without any preheating.

For the experiments incorporating *in situ* CHS of nano-catalyst during the gasification process, the precursor metal salt was dissolved in the biomass solution and then pumped upwards into the reactor. Combined

with the supercritical water, the mixed feed streams flowed upwards into the outer tube of the reactor's annulus configuration. The mixing of the upwards flow (the biomass wastewater with dissolved precursor metal salt and H₂O₂ solution if partial oxidation was included in the experiment) at 10 mL/min and downwards flow (supercritical water) at 10 mL/min occurs just below the nozzle tip of the inner tube (Fig. S2) facilitating nano-catalyst synthesis.

The reactor effluent then flowed out of the side arm of the reactor to the counter-current annulus heat exchanger. After cooling, the product stream was cooled to ambient temperature and then passed through the back pressure regulator, where the gas and liquid products were separated in a gas-liquid separator at ambient conditions. A gas pump was used to assist in the delivery of the gas product from the separator to a Tedlar bag. The gas compositions along the continuous run were measured and analysed every 5 min with the gas analysers (Riken Keiki, Model GX-6000 and Model GX-3R). The gas products collected in the Tedlar bags were analysed immediately after the completion of each run.

The liquid product containing solids was centrifuged (Hettich® ROTOFIX 32A centrifuge) at 4000 rpm for 30 min to separate the solid product (nano-catalyst and tar) and liquid product. COD and TOC levels in the liquid product were also analysed. The solid product was washed with excess acetone, followed by two water washes to recover the nano-catalyst. The recovered nano-catalyst was dried in an oven at 80 °C overnight. Residual H₂O₂ has been previously linked to an over-estimation of COD [35]. Therefore, blank tests were carried out to ensure that all H₂O₂ was consumed within the reactor.

2.5. Characterisation of the nano-catalysts

Samples of the nano-catalyst were prepared using deionised water for examination by transmission electron microscopy (TEM). A drop of this suspended solution mixture was placed on the TEM grid. TEM images were obtained using a JEOL 2100F (FEGTEM) operating with an acceleration voltage of 100 kV. The TEM images were analysed with ImageJ software and more than 150 particles were selected for the determination of particle size. X-ray Diffraction (XRD) analysis was carried out on the dried metal oxide nanoparticles. The analysis was completed using Bruker D8 Advance (Bruker AXS, Germany) using Cu Kα radiation (λ = 1.54 Å) in a 2θ range between 10° and 80°.

2.6. Calculations

The yield of the nano-catalyst, residence time (τ) [15,36], oxidation coefficient (η) [20,37,38], gasification mass efficiency (GE) [39], hydrogen molar selectivity (HS) [39], COD reduction efficiency and TOC reduction efficiency are defined as follows:

$$\text{Yield of nano-catalyst (\%)} = \frac{\text{mass of metal in the recovered nano-catalyst}}{\text{mass of metal in the precursor metal salt solution}} \times 100\% \quad (6)$$

$$\tau = \frac{V_r \cdot \rho_{T,P}}{\varphi_{m,STP}} \quad (7)$$

Where V_r is the reactor's geometric volume, $\rho_{T,P}$ is the average water density at reaction conditions calculated by using Van der Waals equation of state and $\varphi_{m,STP}$ is the total mass flow rate.

$$\eta = \frac{O_2 \text{ from the completed decomposition of } H_2O_2}{\text{theoretically required } O_2 \text{ for the complete oxidation of COD}} \quad (8)$$

$$GE = \frac{\text{mass flow of produced gases } (\frac{kg}{h})}{\text{mass flow of dry matter in feedstock } (\frac{kg}{h})} \times 100 \quad (9)$$

$$HS = \frac{\text{moleflowofH}_2\text{inproducedgases}(\frac{\text{mol}}{\text{h}})}{\text{sumofmoleflowofothergaseousproducts}(\frac{\text{mol}}{\text{h}})} \quad (10)$$

$$\text{COD/TOCreductionefficiency}(\%) = \frac{\text{COD/TOC}_{\text{inlet}} - \text{COD/TOC}_{\text{treatedwater}}}{\text{COD/TOC}_{\text{inlet}}} \times 100 \quad (11)$$

3. Results and discussion

3.1. Characterisation of the biomass wastewaters

The filtered wastewater prior to treatment is shown in Fig. S3(a). The characterisation results are presented in Table 1. The three wastewater feedstocks have COD values greater than 50 g/L and TOC values greater than 10 g/L, which verifies the presence of high organic content in each wastewater.

3.2. The effect of feedstock concentrations

Using olive wastewater as feedstock without partial oxidation, Fig. 1 and Fig. 2 (Table S1) summarise the response of the gas yields, hydrogen selectivity, gasification mass efficiency (GE) and COD reduction efficiency to feedstock concentrations and *in situ* CHS of three metal oxide nano-catalysts, i.e. aluminium hydroxide oxide (AlOOH), cerium(IV) oxide (CeO₂), iron(III) oxide (Fe₂O₃) nano-catalysts.

Under non-catalytic conditions (please see Table S1), the hydrogen yield for 78 g/L COD feedstock was 0.4 mol/kg biomass which was only slightly higher than the hydrogen yield (~0.0 mol/kg) for the 38.6 g/L COD feedstock. The hydrogen yield is mainly attributed to the steam reforming reactions (1) and (2) without the presence of a catalyst in the process [40,26]. By referring to reactions (1) and (2), the mole ratio of hydrogen production is controlled by the organic compounds (C_xH_yO_z) in the feedstock. The 78 g/L COD feed contains a higher concentration of organic compounds which leads to the observation of a slightly higher hydrogen yield than the 38.6 g/L COD feed. It is likely that the 38.6 g/L COD feedstock generates a small amount of hydrogen, which then reacts with CO₂/CO through the methanation reactions (4)–(5) to form methane, producing an elevated CH₄ yield at 0.9 mol/kg biomass compared to 0.6 mol/kg biomass as for the 78 g/L COD feed as per the governing equilibrium driving force. As a consequence, the CO₂ yield is lower at 7.1 mol/kg biomass compared to 9.4 mol/kg biomass, as observed for the 78 g/L COD feed.

The effect of feedstock concentration on the gas yield was investigated using a two-to-fourfold dilution of the raw olive wastewater to obtain a COD in the range of 72.5 to 80.3 g/L (average COD was 78.0 g/L ± 2.5) and 37.7 to 39.2 g/L (average COD was 38.6 g/L ± 0.5). For both

Table 1
Characterisation results of the filtered biomass wastewater.

Parameters	Olive wastewater	Spent lees	Stillage
Colour	Black	Dark Brown	Brown
pH	4.2	5.9	3.4
Moisture content (wt%)	87.9 ± 0.8	98.2 ± 0.7	76.2 ± 0.3
TSS (g/L)	2.3	1.5	44.2
TDS (g/L)	119.2	9.6	118.9
<i>Filtrate</i>			
COD (g/L)	154.3 ± 3.4	50.9 ± 2.2	217.4 ± 3.2
TOC (g/L)	37.5 ± 0.2	10.9 ± 0.5	60.2 ± 1.4
Volatile matters (wt%, dry)	91.0 ± 2.2	80.4 ± 0.8	83.4 ± 1.0
Fixed carbon (wt%, dry)	4.7 ± 0.8	10.7 ± 0.8	12.1 ± 1.0
Ash (wt%, dry)	4.3 ± 1.1	9.0 ± 0.1	4.5 ± 1.9
C (wt%)	37.5	39.6	41.8
H (wt%)	6.4	6.3	7.2
O (wt%)	54.5	53.1	47.2
N (wt%)	1.2	0.7	3.2
S (wt%)	0.4	0.3	0.7

the high and low COD concentrations, the nano-catalyst promoted the gasification reactions compared to the non-catalysed control, where Fe₂O₃ improved the gasification mass efficiency most appreciably for both COD concentrations. Under catalytic conditions, the hydrogen selectivity was greater for the AlOOH and CeO₂ nano-catalysts at the lower COD concentration, whereas the Fe₂O₃ nano-catalyst produced comparable hydrogen selectivity at both CODs. It is plausible that the higher water content in the feedstock with a lower COD (4x dilution) promoted steam reforming and WGS reactions more readily.

3.2.1. Characterisation of the recovered nano-catalysts

Control experiments were conducted by dissolving the precursor metal salt in water (without the flow of the wastewater into the process) for the synthesis of the nano-catalyst only (without gasification reactions). SCWG experiments with the *in situ* formation of nano-catalyst (without partial oxidation) immediately followed control experiments with the introduction of the wastewater flow into the reactor (see Section 2.4). The nano-catalysts from the control and SCWG experiments were recovered after the process and characterised via XRD analysis.

Fig. 3 shows the representative XRD profiles for each control experiment (without gasification reactions) and post-reaction (involved in the gasification reactions, obtained from the SCWG experiment) recovered nano-catalyst, confirming that the obtained pre-reaction and post-reaction nanoparticles were AlOOH, CeO₂ and α-Fe₂O₃. The XRD results also revealed that the recovered nano-catalysts had not been irreversibly fouled by contaminants (such as tar), given all the identified peaks corresponded to the nano-catalyst's identity.

TEM images of each nano-catalyst are shown in Fig. S4 for AlOOH, Fig. S5 for CeO₂ and Fig. S6 for α-Fe₂O₃. The morphology and particle size of each nano-catalyst appear to be quite different. The Fe₂O₃ nano-catalyst showed the smallest particle size with average particle size (32 ± 8 nm) and most of the nanoparticles were spherical-shaped [41]. The TEM images show that most of the Fe₂O₃ nanoparticles were reasonably dispersed, while some of the AlOOH and CeO₂ tended to aggregate together. The TEM samples were prepared by drying out particles in suspension and therefore may or may not indicate that aggregation of AlOOH and CeO₂ occurred during SCWG. Smaller particle sizes have a higher surface area and may therefore give rise to a higher catalytic activity thereby improving gasification [42]. The smaller particle size distribution and possibly more dispersed Fe₂O₃ nano-catalyst promoted a higher gasification efficiency than AlOOH and CeO₂.

3.3. The impact of *in-situ* CHS of metal oxide nano-catalyst

Given the comparable catalytic gasification mass efficiency at the lower and higher COD in Section 3.2, the lower COD wastewater feedstock (38.6 g/L) was used for nano-catalyst studies as it avoided solubility limitations of the metal precursors prior to the reaction. As shown in Fig. 2, catalytic SCWG increased the hydrogen yields significantly from 0.0 to 1.0–1.4 mol/(kg biomass), and enhanced the methane yields moderately from 0.9 to 1.1–1.2 mol/(kg biomass). There was also an improved gasification mass efficiency from 6.2 to 17.6 wt% compared to non-catalytic SCWG (Fig. 1). These results indicate that the nano-catalyst plays an important role in promoting the methanation and water gas shift reactions. Similarly, Cao et al. (2020) studied the catalytic activity of 14 metal oxides during SCWG of black liquor at 600 °C and showed that all the metal oxides improved the hydrogen and methane yields and the gasification efficiency [5]. Cao also concluded that metal oxides present catalytic active sites that promote wastewater decomposition whilst enhancing gasification. Another study with 12 types of metal oxides in SCWG of glucose at 600 °C showed similar findings [43].

The efficiency of nano-catalysts, in terms of hydrogen and methane yields and gasification mass efficiency, showed Fe₂O₃ > CeO₂ > AlOOH. The sequence for the yields of recovered nano-catalysts was in the order of Fe₂O₃ (70.7 %) > CeO₂ (61.9 %) > AlOOH (55.6 %). Iron-based

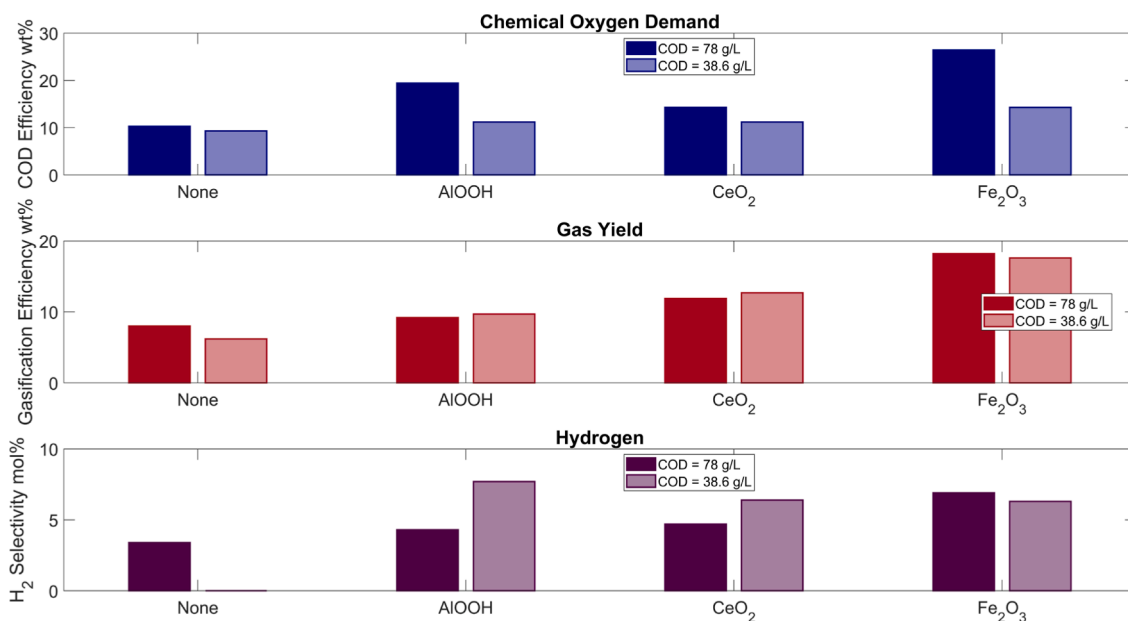


Fig. 1. SCWG of olive wastewater without oxidant co-feed, showing the response to feedstock concentration and type of nano-catalysts on production efficiency at fixed operating condition of $T = 430\text{ }^{\circ}\text{C}$, $P = 235\text{ bar}$, residence time = 20 s with a flow ratio of 1:1, precursor solution concentration = 40 mM (see [Table S1](#) for raw data).

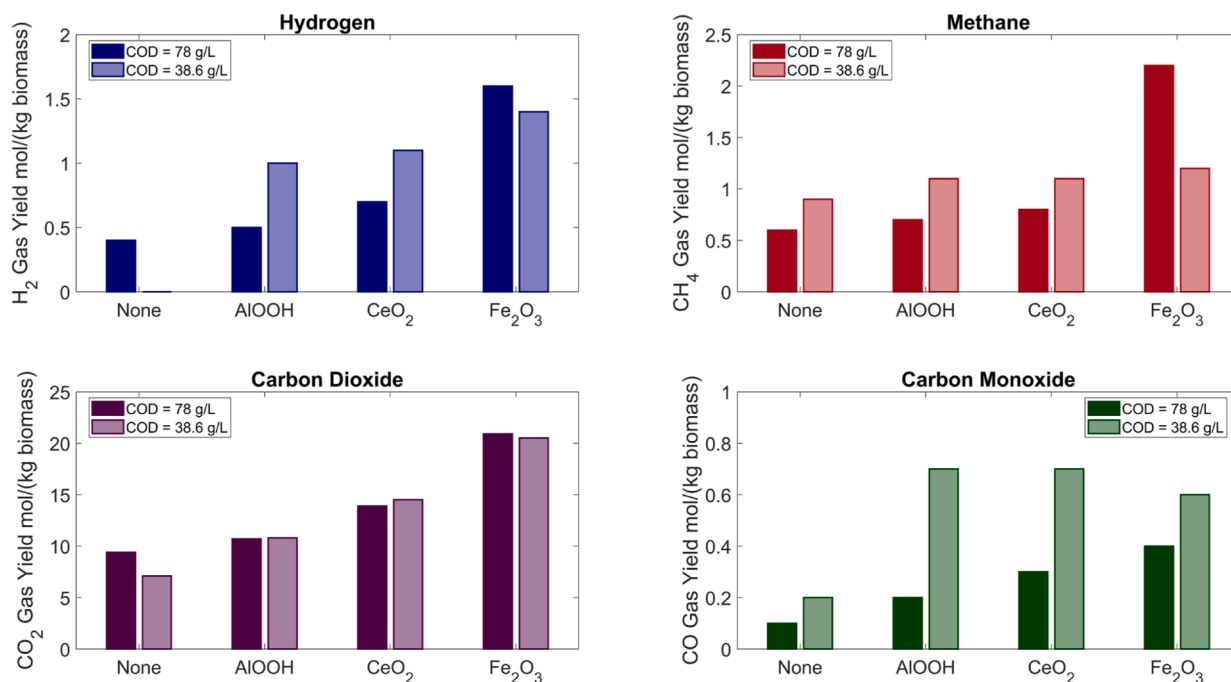


Fig. 2. SCWG of olive wastewater without oxidant co-feed, showing the response to feedstock concentration and type of nano-catalysts on gas yields at fixed operating condition of $T = 430\text{ }^{\circ}\text{C}$, $P = 235\text{ bar}$, residence time = 20 s with a flow ratio of 1:1, precursor solution concentration = 40 mM (see [Table S1](#) for raw data).

catalysts, particularly iron oxide, have been widely studied for biomass conversion recently and promising results have been reported [44]. Cao et al. (2020) also found that Fe₂O₃ was superior to CeO₂ and Al₂O₃, in terms of hydrogen yield and gasification efficiency [5].

Furthermore, the bulk price of Fe(NO₃)₃·9H₂O (USD 500/tonne), which is the precursor to synthesise Fe₂O₃, is more cost-effective than Al(NO₃)₃·9H₂O (USD 650/tonne) and Ce(NO₃)₃·6H₂O (USD 1500/tonne), which are the precursors to synthesise AlOOH and CeO₂. The impact of CeO₂ on the environment (and human health) remains uncertain, given a study [45] has shown that CeO₂ nanoparticles potentially yield

negative impacts on human health and the ecosystem, but another study [46] reported that its environmental risk in the marine environment appears low. For aluminium compounds, a study [47] revealed that aluminium oxides, hydroxides and oxyhydroxides have not been classified with respect to carcinogenicity; however, occupational limits exist in several countries for exposures to aluminium dust and aluminium oxide. The environmental risk of iron oxide nanoparticles remains an open question, as a few studies indicated that the release of iron oxide nanoparticles into the environment may be harmful to various eco-relevant organisms [48–50] even though its low toxicity has been

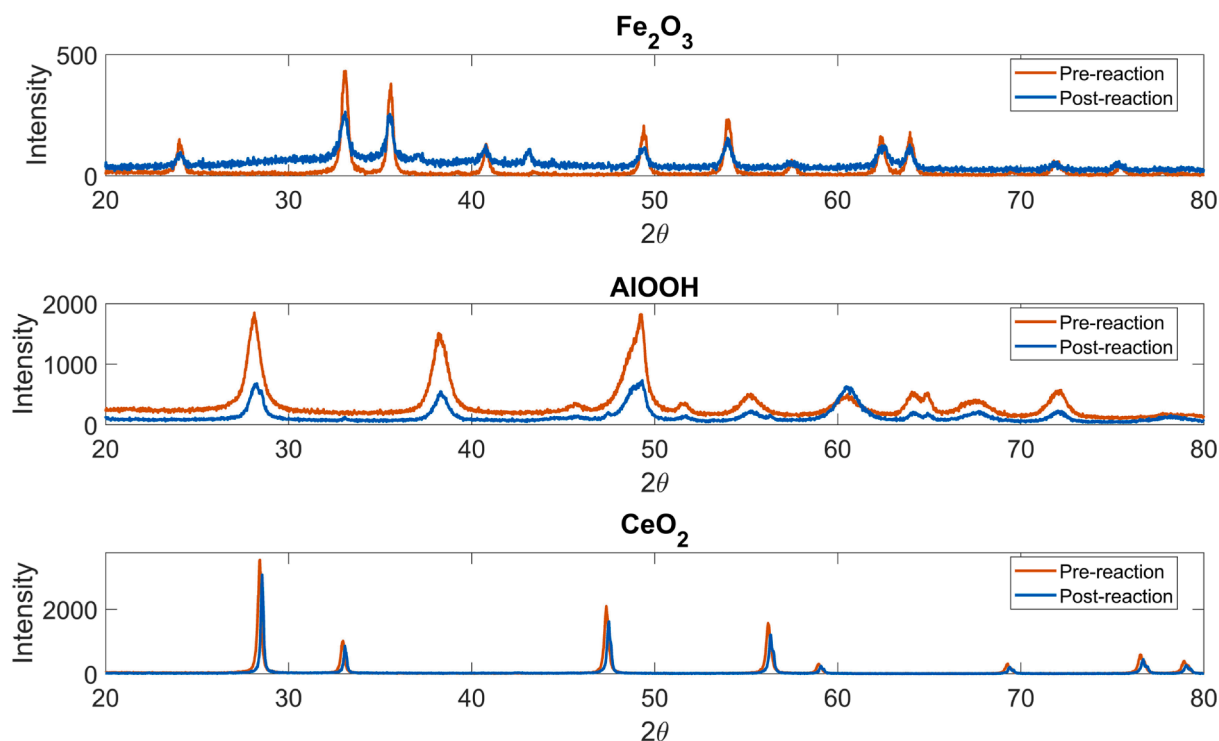


Fig. 3. XRD profiles of pre-reaction and post-reaction recovered nano-catalysts.

reported [51].

Given the superior gasification efficiency of the Fe_2O_3 nano-catalyst in Fig. 1 and Fig. 2, the Fe_2O_3 nano-catalyst was selected for the subsequent SCWG studies. The next study investigated the impact of using partial oxidation (through the addition of H_2O_2 as an oxidant) to improve the efficiency of the catalytic SCWG process.

3.4. The impact of adding an oxidant (partial oxidation) to the catalytic SCWG process

Using olive wastewater as the feedstock, the effect of adding varying amounts of H_2O_2 as a partial oxidant into the catalytic (Fe_2O_3) SCWG process was investigated. The results are presented in Fig. 4 for production efficiency and Fig. 5 for gas yields (Table S2).

The results revealed that the addition of H_2O_2 at $\eta = 0.4$ into the catalytic process has no appreciable effect on hydrogen and methane yields but enhanced the COD reduction efficiency from 14.3 to 44.6 wt

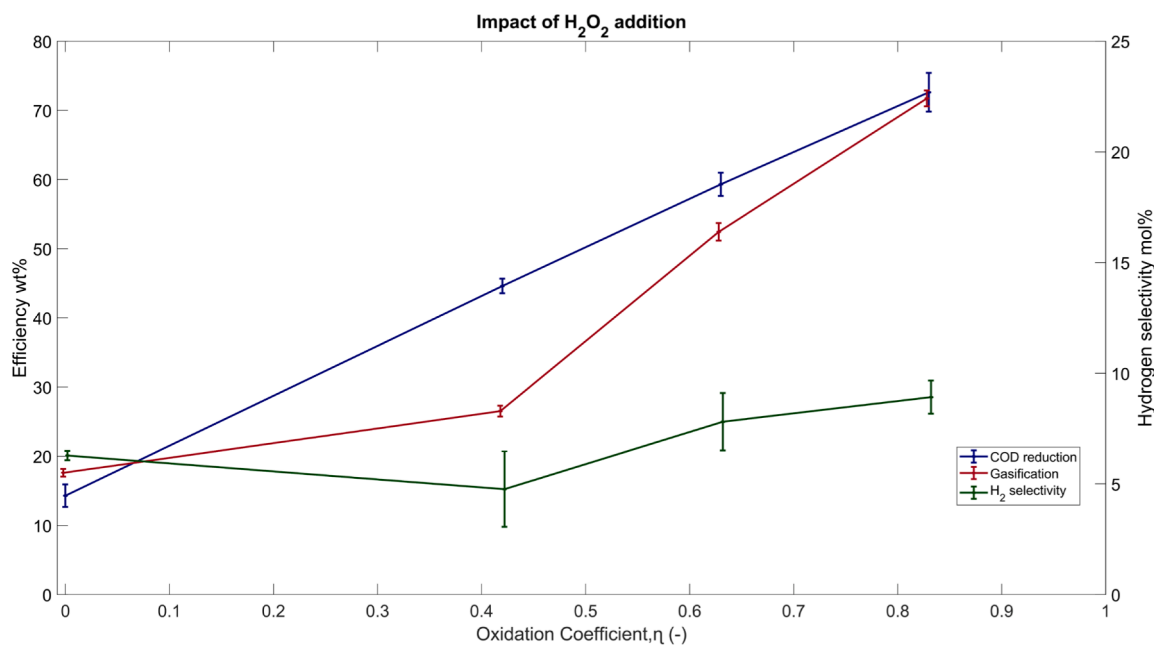


Fig. 4. The effect of adding H_2O_2 into the catalytic SCWG process on production efficiency using fixed operating conditions: $T = 430^\circ\text{C}$, $P = 235$ bar, residence time = 20 s with a flow ratio of 1:1, precursor solution concentration = 40 mM, feedstock concentration = 38.6 g/L COD (see Table S2 for raw data).

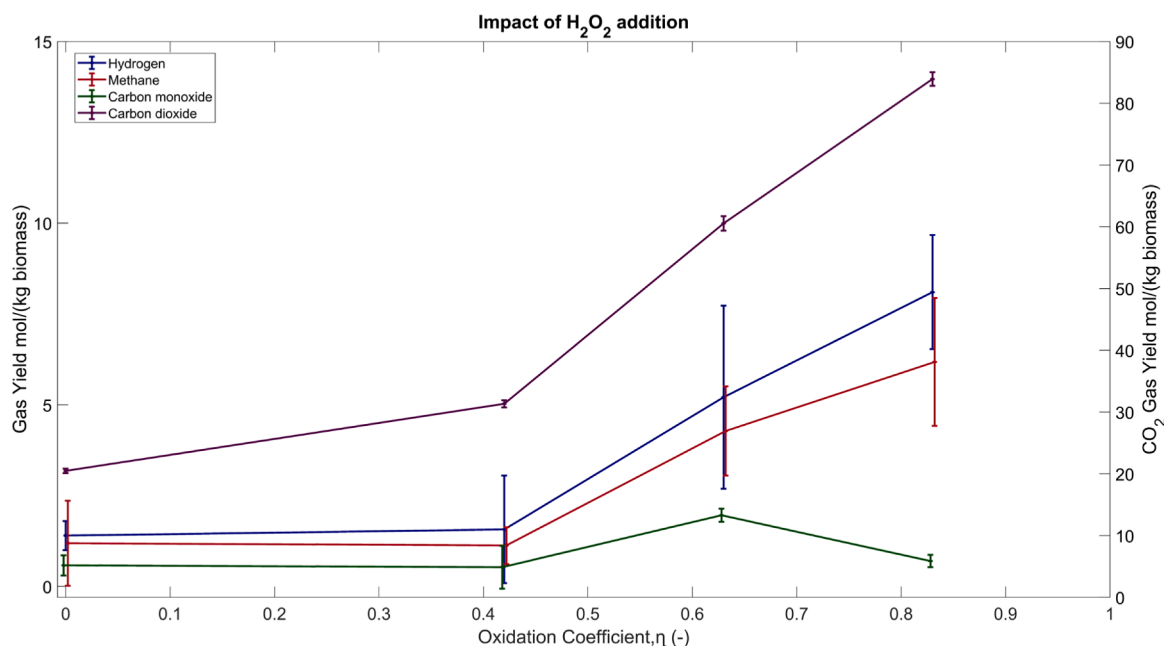


Fig. 5. The response to H_2O_2 addition into the catalytic SCWG process on gas yields using fixed operating conditions: $T = 430\text{ }^\circ\text{C}$, $P = 235\text{ bar}$, residence time = 20 s with a flow ratio of 1:1, precursor solution concentration = 40 mM, feedstock concentration = 38.6 g/L COD (see Table S2 for raw data).

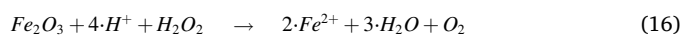
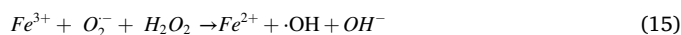
%. However, by increasing the oxidation coefficient to $\eta = 0.6$, the hydrogen and methane yields were increased from 1.4 to 5.2 mol/(kg biomass) and 1.2 to 4.3 mol/(kg biomass) respectively. In addition, COD reduction efficiency increased from 44.6 to 59.3 wt%. Further increasing the oxidation coefficient to $\eta = 0.8$, improved the hydrogen and methane yields from 5.2 to 8.1 mol/(kg biomass) and 4.3 to 6.2 mol/(kg biomass) respectively. COD reduction efficiency was also increased from 59.3 to 72.6 wt%. In all cases, hydrogen selectivity was not significantly impacted. This suggests that raising η provides free radicals that improve the decomposition rate of the organic compounds, facilitating gasification and oxidation reactions [22,20]. A similar trend was observed in previous SCWG studies that included partial oxidation in the process [23,37].

As per the mechanism outlined in Fig. 6, the results suggest that the iron oxide catalyst facilitates the Fenton depolymerisation of biomass macromolecules. Fe_2O_3 (hematite) facets confine ferrous ions as Fenton catalysts to degrade complex organic macromolecules to lower

molecular weight compounds conducive to the steam reforming reactions (1)–(2) [52], which approach an equilibrium condition dictated by the operating conditions and specie concentrations associated with the reversible reactions (3)–(5). Initiating this decomposition to inorganic C_1 species, for example, lignin is appreciably depolymerised by hydroxyl radicals through cleavage of β -ether bonds between lignin residues [53,54]. The Fenton reaction (12) plays a central role in generating the necessary hydroxyl free radical species.



Additionally, given the low pH of olive wastewater and the iron oxide catalyst [55], heterogeneous surface Fe^{3+} adjacent to adsorbed H^+ can be reduced by adsorbed H_2O_2 , inducing H_2O_2 decomposition to adsorbed $\cdot OOH$; desorbing from the heterogeneous surface as Fe^{2+} (reaction (13)). The adsorbed H^+ promotes the formation of the superoxide free radical as per reaction (14), which in turn can promote further H_2O_2 decomposition leading to the generation of $\cdot OH$ (reaction (15)). These Haber-Weiss reactions contribute to reducing the ferric ions produced by reaction (12) in a cyclical manner to ferrous ions, thereby enabling continued oxygen free-radical species synthesis. The overall heterogeneous reaction may be described by reaction (16).



Contributing to the cyclical generation of free radicals, at temperatures below $570\text{ }^\circ\text{C}$, the Fe_2O_3 (hematite) can be reduced to Fe_3O_4 (magnetite) by H_2 as in the reversible reaction (17) [56].



Whereas Fe_2O_3 nanoparticles were recovered from the SCWG without partial oxidation, the recovered nano-catalyst after SCWG with partial oxidation was confirmed by XRD to be Fe_3O_4 (Fig. S7). The SCWG reaction environment with partial oxidation was thus, on balance, more reducing than without partial oxidation. The formation of magnetite

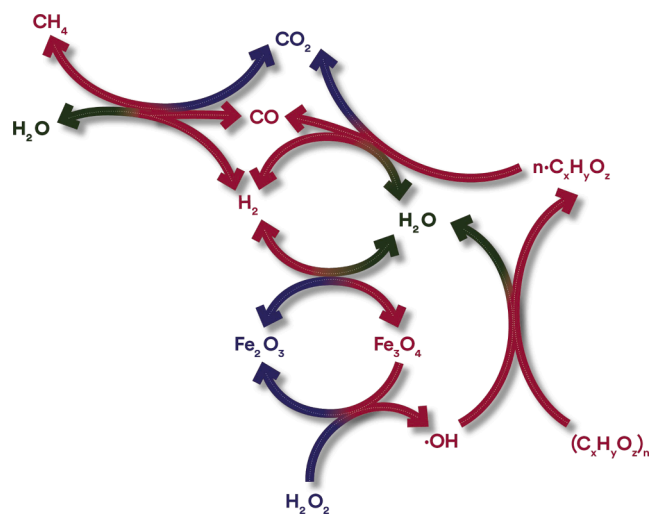


Fig. 6. Supercritical water gasification mechanism, illustrating the interplay between the oxidant, iron oxide catalyst and the gasification reactions.

provides an opportunity to recover the nanoparticles from the process using an electromagnet, as a co-product and to avoid environmental release (see Section 3.3).

H₂O₂ addition where $\eta \geq 1$ (oxidant supply is greater than theoretical demand) was not investigated, as excess oxidant would inevitably convert hydrogen and methane to water and CO₂ [57]. Partial oxidation, at 430 °C, with *in situ* nano-catalyst formation was demonstrably effective at improving the hydrogen and methane yields, gasification, and COD reduction efficiencies with olive wastewater as the feedstock.

3.5. The effect of Fe₂O₃ nano-catalyst precursor concentration

The effect of *in situ* Fe₂O₃ nano-catalyst concentrations on the gas yields and production efficiency was studied at four different precursor solution concentrations (0, 20, 40 and 60 mM) and the results are presented in Fig. 7 and Fig. 8 (Table S3). A concentration of 60 mM was selected as the upper limit because higher concentrations led to a more viscous feedstock, possibly through limitation in precursor solubility or the initiation of a reaction between the precursor and the olive wastewater.

At a constant oxidation coefficient of $\eta = 0.8$, the increase in precursor concentration from 0 – 60 mM had minimal impact on the gasification mass efficiency, though the COD reduction efficiency was significantly increased from 53.3 to 72.6 wt% (Fig. 7). Hydrogen and methane yields were dramatically increased from 3.3 to 9.6 mol/(kg biomass) and 2.7 to 6.6 mol/(kg biomass) respectively, increasing the hydrogen selectivity from 7.9 to 11.0 mol%.

The iron oxide nano-catalyst appreciably promotes the steam reforming reactions that decompose the organic molecules to yield inorganic gas products, whilst also promoting the WGS over the methanation reaction. Based on the results, it appears that the impact of metal oxide on the gasification reactions is more pronounced at < 40 mM precursor concentration. Precursor concentrations greater than 40 mM appear to have a non-linear influence on the gas concentration, plausibly increasing the consumption of H₂ as per reaction (17). Similar findings have been reported in a study that investigated the influence of the loading amount of V₂O₅ [vanadium(V) oxide] on the SCWG of black liquor [5]. Increasing the V₂O₅ catalyst loading to < 45 wt% improved the hydrogen production and gasification efficiency significantly, but

the hydrogen fraction decreased when the V₂O₅ loading was >45 wt%.

3.6. Comparison of different wastewater feedstocks

In summary, optimised conditions for hydrogen and methane generation from olive wastewater appear to be $\eta = 0.8$, feedstock concentration of 38.6 g/L COD and 60 mM precursor solution concentration; promoted by the *in situ* formation of Fe₂O₃ nano-catalyst at T = 430 °C, P = 235 bar, residence time = 20 s with a flow ratio of 1:1. Three different wastewater feedstocks were tested for comparison at these conditions with three notable adjustments: spent lees was diluted 2 times and stillage was diluted 4 times before it was used. Furthermore, a catalyst precursor concentration of 40 mM was selected to avoid solubility challenges observed in spent lees and stillage at 60 mM. The results are presented in Fig. 9 and Fig. 10 (Table S4).

Fig. S3 compares the wastewater colour before and after the SCWG-CHS process with partial oxidation for each wastewater under the optimised conditions. After the process, the colour of the stillage changed from brown to yellow, meanwhile, the colour of the spent lees was changed from dark brown to colourless and the colour of the olive wastewater was changed from black to yellow. This decolouration effect is likely due to the biomass decomposition/degradation and conversion to syngas caused by the Fenton oxidation reaction and gasification reactions described in Section 3.4.

Fig. S8 summarises the study results in four dimensions, where the three cartesian axes are feed COD, precursor concentration and oxidation coefficient and the colour heat map represents the H₂ and CH₄ yields along with the gasification and COD reduction efficiencies. Across the three industrial feedstocks, the COD reduction and gasification efficiencies were comparable at high precursor concentrations and high oxidation coefficients. However, H₂ and CH₄ yields were more pronounced for stillage and spent lees than for olive wastewater. In this study, it is postulated that stillage generated the highest hydrogen and methane yields because it contained the highest C (41.8 wt%) and the highest H (7.2 wt%) and the lowest O (47.2 wt%). In contrast, olive wastewater contained the lowest C (37.5 wt%) and the highest O (54.5 wt%) content and generated the lowest hydrogen and methane yields.

An experimental continuous SCWG study that operated at 600 °C, 350 bar and 8 wt% biomass feedstocks (using tomato residue, hazelnut

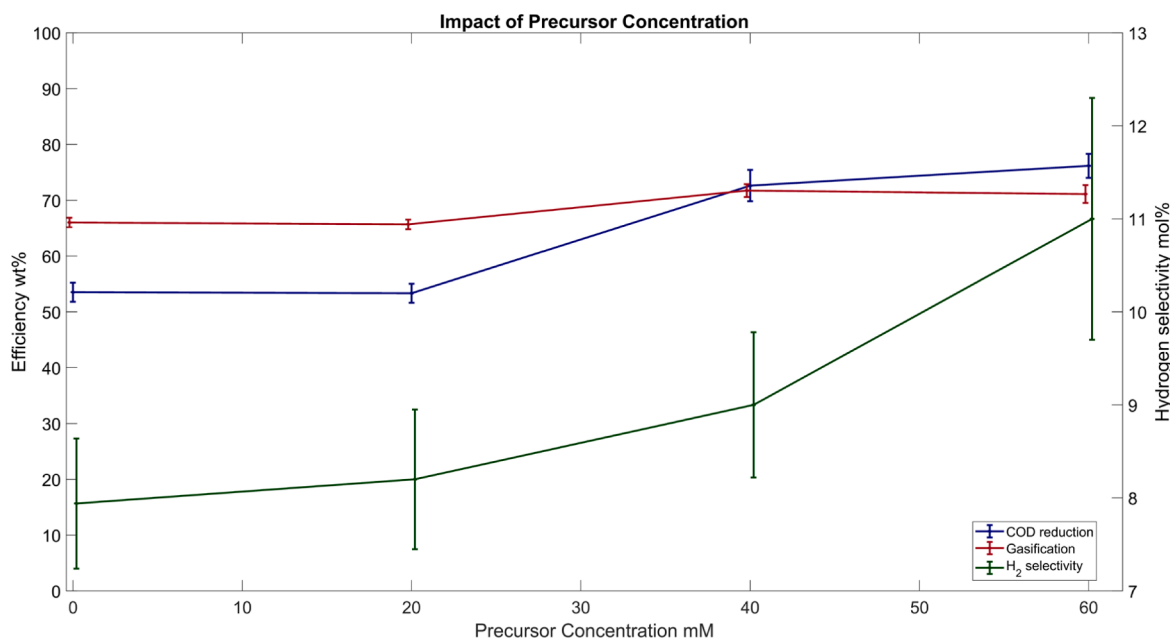


Fig. 7. The effect of precursor feed concentration on production efficiency at fixed operating conditions: T = 430 °C, P = 235 bar, residence time = 20 s with a flow ratio of 1:1, feedstock concentration = 38.6 g/L COD, $\eta = 0.8$ (see Table S3 for raw data).

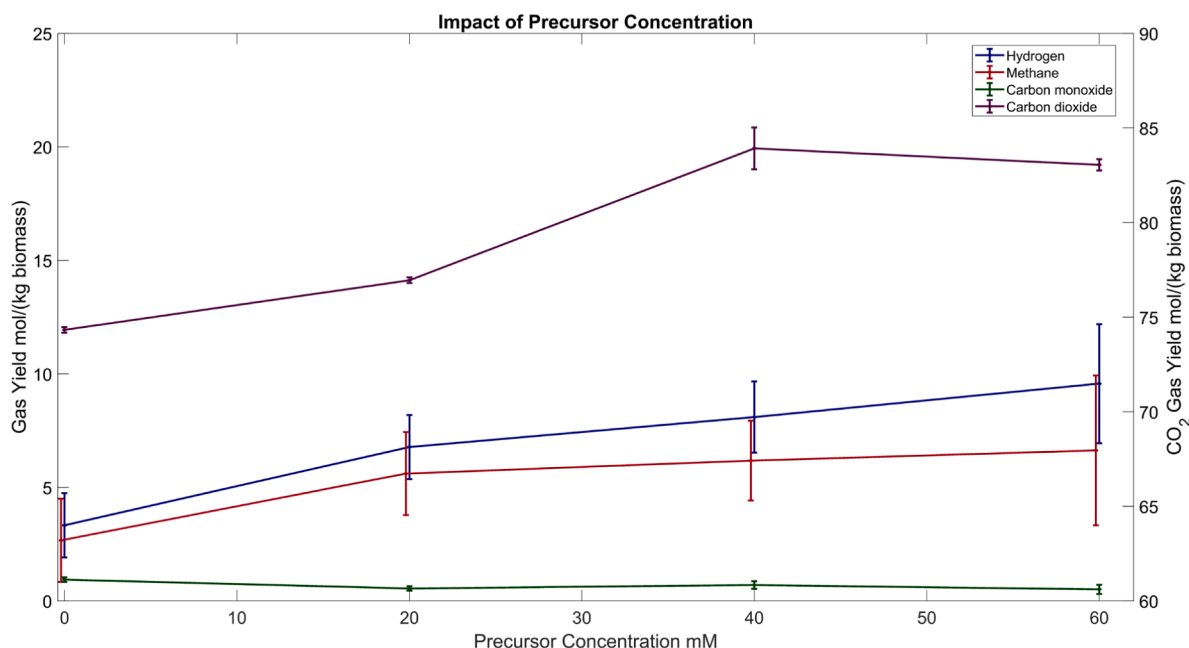


Fig. 8. The effect of precursor feed concentration on gas yields at fixed operating conditions: $T = 430\text{ }^{\circ}\text{C}$, $P = 235\text{ bar}$, residence time = 20 s with a flow ratio of 1:1, feedstock concentration = 38.6 g/L COD, $\eta = 0.8$ (see Table S3 for raw data).

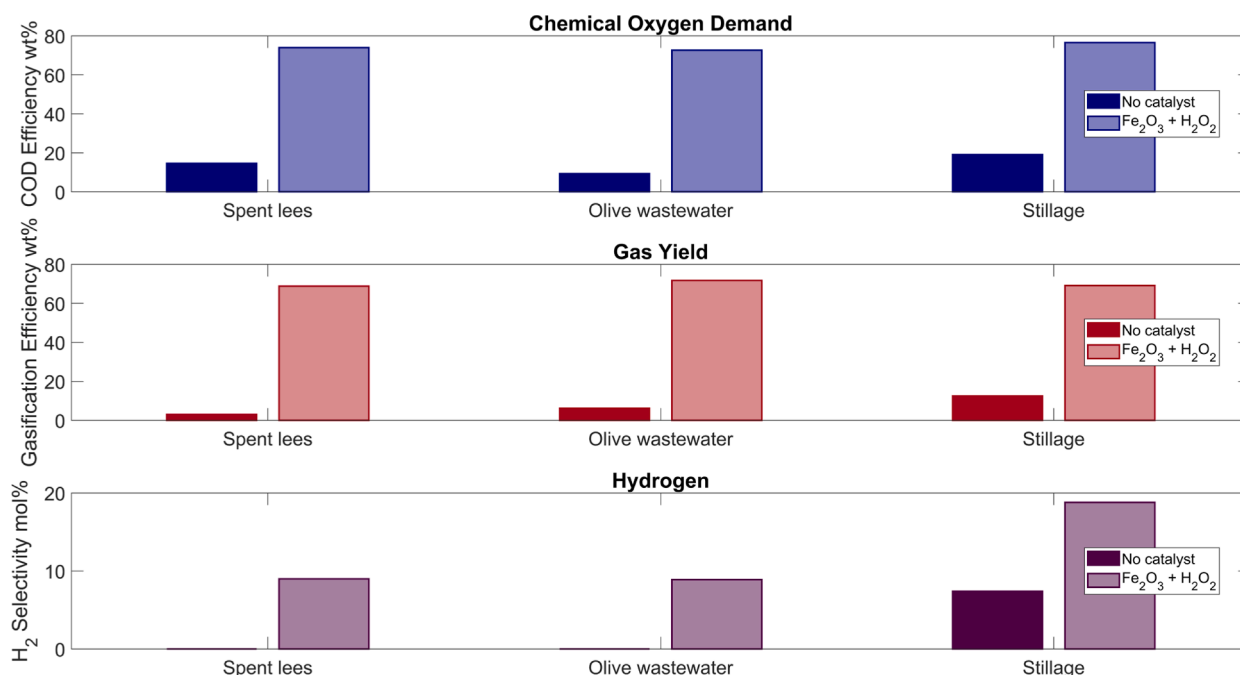


Fig. 9. The comparison between different wastewater feedstocks on production efficiency at fixed operating conditions: $T = 430\text{ }^{\circ}\text{C}$, $P = 235\text{ bar}$, residence time = 20 s with a flow ratio of 1:1, precursor solution concentration = 40 mM, $\eta = 0.8$ (see Table S4 for raw data).

shell, extracted acorn and acorn as feedstocks) also reported that biomass containing higher C and H and lower O tended to produce the highest hydrogen and methane yields [58]. Tomato residue had the highest C (54.7 wt%) and H (7.6 wt%) content and the lowest O (31.7 wt%), surpassing all other biomasses to produce the highest hydrogen (17.9 mol/kg C in feed) and methane (16.5 mol/kg C in feed) yields. A similar finding was reported in another experimental study at 600 °C, 230 bar and 1:10 biomass-to-water mass ratio using fruit wastes and agri-food residues as the feedstocks [59]. Their results revealed that the highest hydrogen yield (2.2 mol/kg biomass) was achieved from

coconut shell that contains high C but low O levels.

3.7. The impact of time on gasification performance for different wastewater feedstocks

Previous SCWG experiments have reported rapid catalyst deactivation owed to charring and sintering, particularly when employing fixed bed configurations, often within minute timescales [28–30]. Assessing stable steady state operation, the continuous gasification of olive wastewater, spent lees and stillage feedstocks was monitored for 40 min

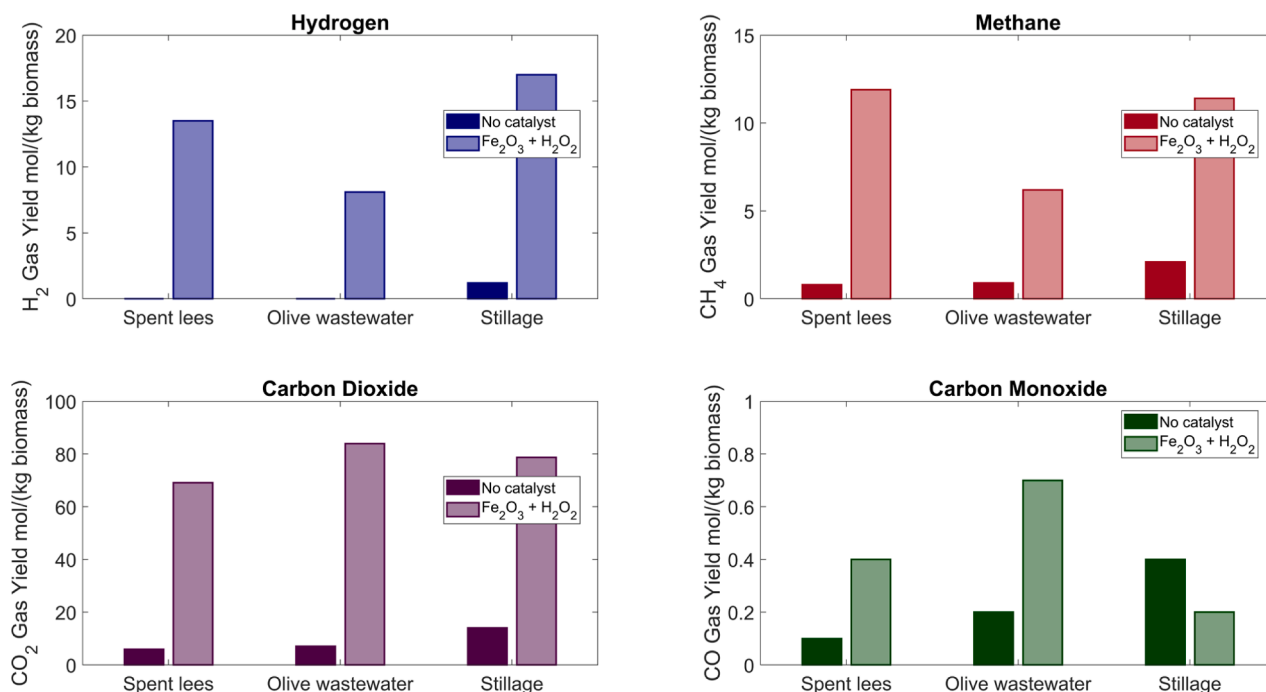


Fig. 10. The comparison between different wastewater feedstocks on gas yields at fixed operating conditions: $T = 430\text{ }^{\circ}\text{C}$, $P = 235\text{ bar}$, residence time = 20 s with a flow ratio of 1:1, precursor solution concentration = 40 mM, $\eta = 0.8$ (see Table S4 for raw data).

using gas yields as the response factor. The hydrogen and methane yields are presented in Fig. S9.

Fig. S9 shows that the hydrogen and methane yields generated from different wastewater feedstocks were maintained at a steady state without significant performance drop during the 40 min continuous experiment. These results indicate that combining continuous SCWG with *in situ* CHS of Fe₂O₃ nano-catalyst and partial oxidation can maintain stable gasification performance.

3.8. Comparison of the results from this work with the literature

The optimised results from this work in terms of gas yields and TOC reduction efficiency were compared with similar processes under continuous flow from the literature that similarly used olive wastewater as the feedstock and the comparison is presented in Table S5.

A direct comparison of this work with results in the literature cannot be made due to the feedstock originating from different sources, set against further differences in reactor geometry and operating conditions (including reaction time and catalyst type). However, general observations can be made. The comparison results in Table S5 show hydrogen (9.6 mol% versus 7.3–8.0 mol%) and methane (6.7 mol% versus 2.1–2.4 mol%) yields and the TOC reduction efficiency (55.0 wt% versus 12.0–46.2 wt%) are higher with our combined approach than a process that uses Ni/Al₂O₃ as the catalyst [14] or other approaches that use H₂O₂ + O₂ as the oxidant [25]. Methane yield and the TOC reduction efficiency appear to be higher if using Ru/Al₂O₃ as the catalyst [14], but our hydrogen yield (9.6 versus 5.2 mol%) is notably higher and with a significantly shorter reaction time (20 s versus 30 s). Furthermore, the iron-based catalyst synthesised in this study is more cost-effective [60] than, for example, a fixed-bed ruthenium-based catalyst used in the literature [14].

A further comparison was made by comparing gas yields and COD/TOC reduction efficiencies from this study to selected SCWG studies from the open literature with the other types of wastewater feedstocks across a wide temperature range from 450 to 675 °C. Results are shown in Table S6. Table S6 shows that combining continuous SCWG with *in situ* CHS of Fe₂O₃ nano-catalyst and partial oxidation produces

favourable hydrogen and methane yields, alongside significant reductions in COD attributed to partial oxidation. These results were obtained using significantly lower operating temperature (430 °C versus 450–675 °C) and shorter reaction time (20 s versus 150–3600 s) than reported by the studies highlighted in Table S6, supporting a reduced capital burden owed to the lower required reactor volume and energy.

4. Conclusions

This paper presents a novel continuous hydrothermal process that integrates SCWG with *in situ* synthesis of fresh metal oxide nano-catalyst at low operating temperature (430 °C). Industrial biomass wastewater was used as the feedstock for generating hydrogen and methane-rich syngas, with a metal oxide nano-catalyst as a valuable co-product and cleaner water, lower in COD and TOC, as a liquid product. For the generation of hydrogen and methane from olive wastewater, optimised conditions were shown to be 430 °C, 235 bar and a residence time of 20 s with a flow ratio of 1:1 were (1) $\eta = 0.8$, (2) feedstock concentration of 38.6 g/L COD and (3) a precursor concentration of 60 mM for the *in situ* synthesis of Fe₂O₃ nano-catalyst.

Operating at these optimised operating conditions, stillage showed the highest performance in terms of hydrogen [17 mol/(kg biomass)] and methane [11.4 mol/(kg biomass)] yields, hydrogen selectivity (18.8 %) and COD reduction (76.5 %) efficiency, followed by spent lees and olive wastewater. This process managed to achieve gasification, COD and TOC reduction efficiencies in the range of 68.8–71.7 %, 72.6–76.5 % and 53.9–55.7 % respectively. A comparison of the optimised experimental results from this study with the open literature demonstrated that this process is efficient for generating syngas high in hydrogen and methane from different types of biomass wastewater, whilst concurrently reducing the COD and TOC.

In addition, this process was further validated by showing stable, steady-state gasification performance in terms of gas yields with olive wastewater, stillage and spent lees as the feedstocks during continuous operation for 40 min without any significant drop in performance. Lastly, the design of this process at a low operating temperature ($\leq 430\text{ }^{\circ}\text{C}$) significantly improves its potential to be economically

feasible for the large-scale continuous generation of hydrogen and methane.

5. Recommendations of future work

The future work plan as the extension of this study is listed below.

- The effect of increasing the residence time from 20 s to 50–200 s without the co-feed of oxidant to the process will be investigated to evaluate the possibility of achieving similar gasification efficiency using longer residence times. The economic feasibility of both routes (addition of oxidant to the process with a short residence time, and increased residence time without co-feed of an oxidant) will be evaluated via a techno-economic analysis.
- A modelling study has shown that the integration of SCWG (an endothermic process) with a biorefinery process such as continuous gas fermentation (an exothermic process) is a feasible route to lower the energy costs of SCWG [1]. Future practical work will be conducted to validate the modelling results at bench and pilot scale.

CRedit authorship contribution statement

Chai Siah Lee: Conceptualization, Methodology, Software, Validation, Formal analysis, Investigation, Data curation, Visualization, Project administration, Writing – original draft, Writing – review & editing. **Alex V. Conradie:** Conceptualization, Formal analysis, Visualization, Funding acquisition, Writing – review & editing. **Edward Lester:** Conceptualization, Methodology, Validation, Formal analysis, Resources, Funding acquisition, Writing – review & editing, Supervision.

Declaration of Competing Interest

The authors declare that they have no known competing financial interests or personal relationships that could have appeared to influence the work reported in this paper.

Data availability

Data will be made available on request.

Acknowledgements

The authors gratefully acknowledge all the support received from the University of Nottingham Research Beacon of Excellence: Green Chemicals, technical support from the Advanced Biofuel Solutions Ltd, the wastewater source from the Warner's Distillery Ltd and Sedamyl UK. Finally, the authors would like to express their deep gratitude to the Supergen Bioenergy Hub for providing the Supergen Rapid Response Flexible Funding (grant number: RR 2021_7) and the EPSRC (Grant number EP/R032807/1) in support of this study.

Appendix A. Supplementary data

Supplementary data to this article can be found online at <https://doi.org/10.1016/j.cej.2022.140845>.

References

- R.R. Bommareddy, Y. Wang, N. Percy, M. Hayes, E. Lester, N.P. Minton, A. V. Conradie, A sustainable chemicals manufacturing paradigm using CO₂ and renewable H₂, *IScience*. 23 (2020), 101218, <https://doi.org/10.1016/j.isci.2020.101218>.
- G. Weijin, L. Binbin, W. Qingyu, H. Zuohua, Z. Liang, Supercritical water gasification of landfill leachate for hydrogen production in the presence and absence of alkali catalyst, *Waste Manag.* 73 (2018) 439–446, <https://doi.org/10.1016/j.wasman.2017.12.015>.
- H.T. Nguyen, E. Yoda, M. Komiya, Catalytic supercritical water gasification of proteinaceous biomass: catalyst performances in gasification of ethanol fermentation stillage with batch and flow reactors, *Chem. Eng. Sci.* 109 (2014) 197–203, <https://doi.org/10.1016/j.ces.2014.01.036>.
- H. Boucard, M. Watanabe, S. Takami, E. Weiss-Hortala, R. Barna, T. Adschiri, Beneficial use of CeO₂ nanocatalyst for black liquor conversion under sub and supercritical conditions, *J. Supercrit. Fluids*. 105 (2015) 66–76, <https://doi.org/10.1016/j.supflu.2015.02.008>.
- C. Cao, Y. Xie, L. Mao, W. Wei, J. Shi, H. Jin, Hydrogen production from supercritical water gasification of soda black liquor with various metal oxides, *Renew. Energy*. 157 (2020) 24–32, <https://doi.org/10.1016/j.renene.2020.04.143>.
- A. Loppinet-Serani, C. Reverte, F. Cansell, C. Aymonier, Supercritical water biomass gasification process as a successful solution to valorize wine distillery wastewaters, *ACS Sustain. Chem. Eng.* 1 (2013) 110–117, <https://doi.org/10.1021/sc300058f>.
- C. Wang, W. Zhu, C. Chen, H. Zhang, N. Lin, Y. Su, Influence of reaction conditions on the catalytic activity of a nickel during the supercritical water gasification of dewatered sewage sludge, *J. Supercrit. Fluids*. 140 (2018) 356–363, <https://doi.org/10.1016/j.supflu.2018.07.018>.
- M. Yan, H. Su, Z. Zhou, D. Hantoko, J. Liu, J. Wang, R. Wang, E. Kanchanapit, Gasification of effluent from food waste treatment process in sub- and supercritical water: H₂-rich syngas production and pollutants management, *Sci. Total Environ.* 730 (2020), 138517, <https://doi.org/10.1016/j.scitotenv.2020.138517>.
- P. Casademont, M.B. García-Jarana, J. Sánchez-Oneto, J.R. Portela, E.J. Martínez de la Ossa, Hydrogen production by catalytic conversion of olive mill wastewater in supercritical water, *J. Supercrit. Fluids*. 141 (2018) 224–229, <https://doi.org/10.1016/j.supflu.2017.11.033>.
- E. Adar, M. Ince, M.S. Bilgili, Supercritical water gasification of sewage sludge by continuous flow tubular reactor: a pilot scale study, *Chem. Eng. J.* 391 (2020), 123499, <https://doi.org/10.1016/j.cej.2019.123499>.
- Y. Chen, L. Guo, W. Cao, H. Jin, S. Guo, X. Zhang, Hydrogen production by sewage sludge gasification in supercritical water with a fluidized bed reactor, *Int. J. Hydrogen Energy* (2013), <https://doi.org/10.1016/j.ijhydene.2013.03.165>.
- W. Cao, C. Cao, L. Guo, H. Jin, M. Dargusch, D. Bernhardt, X. Yao, Hydrogen production from supercritical water gasification of chicken manure, *Int. J. Hydrogen Energy*. 41 (2016) 22722–22731, <https://doi.org/10.1016/j.ijhydene.2016.09.031>.
- T. Yanagida, T. Minowa, Y. Shimizu, Y. Matsumura, Y. Noda, Recovery of activated carbon catalyst, calcium, nitrogen and phosphate from effluent following supercritical water gasification of poultry manure, *Bioresour. Technol.* 100 (2009) 4884–4886, <https://doi.org/10.1016/j.biortech.2009.05.042>.
- E. Kıpçak, M. Akgün, Biofuel production from olive mill wastewater through its Ni/Al₂O₃ and Ru/Al₂O₃ catalyzed supercritical water gasification, *Renew. Energy*. 124 (2018) 155–164, <https://doi.org/10.1016/j.renene.2017.06.075>.
- P. Casademont, L. Cardozo-Filho, E. Meurer, J. Sánchez-Oneto, J.R. Portela, Gasification of olive oil mill waste by supercritical water in a continuous reactor, *J. Supercrit. Fluids*. 142 (2018) 10–21, <https://doi.org/10.1016/j.supflu.2018.06.001>.
- E. Kıpçak, O.Ö. Söğüt, M. Akgün, Hydrothermal gasification of olive mill wastewater as a biomass source in supercritical water, *J. Supercrit. Fluids*. 57 (2011) 50–57, <https://doi.org/10.1016/j.supflu.2011.02.006>.
- V. Sricharoenchaikul, Assessment of black liquor gasification in supercritical water, *Bioresour. Technol.* 100 (2009) 638–643, <https://doi.org/10.1016/j.biortech.2008.07.011>.
- C. De Blasio, G. Lucca, K. Özdenkci, M. Mulas, K. Lundqvist, J. Koskinen, M. Santarelli, T. Westerlund, M. Järvinen, A study on supercritical water gasification of black liquor conducted in stainless steel and nickel-chromium-molybdenum reactors, *J. Chem. Technol. Biotechnol.* 91 (2016) 2664–2678, <https://doi.org/10.1002/jctb.4871>.
- W. Gong, Z. Zhou, Y. Liu, Q. Wang, L. Guo, Catalytic gasification of sewage sludge in supercritical water: Influence of K₂CO₃ and H₂O₂ on hydrogen production and phosphorus yield, *ACS Omega*. 5 (2020) 3389–3396, <https://doi.org/10.1021/acsomega.9b03608>.
- L. Qian, S. Wang, S. Wang, S. Zhao, B. Zhang, Supercritical water gasification and partial oxidation of municipal sewage sludge: an experimental and thermodynamic study, *Int. J. Hydrogen Energy*. 46 (2021) 89–99, <https://doi.org/10.1016/j.ijhydene.2020.09.200>.
- Y. Matsumura, M. Harada, D. Li, H. Komiya, Y. Yoshida, H. Ishitani, Biomass gasification in supercritical water with partial oxidation, *J. Japan Inst. Energy*. 82 (2003) 919–925.
- X. Runcheng, L. Yi, B. Tao, Y. Yong, D. Kun, Y. Zhibin, Supercritical water gasification of petrochemical wastewater for hydrogen production, *Environ. Prog. Sustain Energy*. 35 (2016) 428–432, <https://doi.org/10.1002/ep.12253>.
- E.A. Youssef, E. Elbeshbishy, H. Hafez, G. Nakhla, P. Charpentier, Sequential supercritical water gasification and partial oxidation of hog manure, *Int. J. Hydrogen Energy*. 35 (2010) 11756–11767, <https://doi.org/10.1016/j.ijhydene.2010.08.097>.
- M.B. García-Jarana, J. Sánchez-Oneto, J.R. Portela, E. Nebot Sanz, E.J. Martínez de la Ossa, Supercritical water gasification of industrial organic wastes, *J. Supercrit. Fluids*. 46 (2008) 329–334, <https://doi.org/10.1016/j.supflu.2008.03.002>.
- E. Kıpçak, M. Akgün, Oxidative gasification of olive mill wastewater as a biomass source in supercritical water: effects on gasification yield and biofuel composition, *J. Supercrit. Fluids*. 69 (2012) 57–63, <https://doi.org/10.1016/j.supflu.2012.05.005>.
- C.S. Lee, A.V. Conradie, E. Lester, Review of supercritical water gasification with lignocellulosic real biomass as the feedstocks: process parameters, biomass

- composition, catalyst development, reactor design and its challenges, *Chem. Eng. J.* 415 (2021), 128837, <https://doi.org/10.1016/j.cej.2021.128837>.
- [27] J.A. Okolie, R. Rana, S. Nanda, A.K. Dalai, J.A. Kozinski, Supercritical water gasification of biomass: a state-of-the-art review of process parameters, reaction mechanisms and catalysis, *Sustain Energy Fuels*. 3 (2019) 578–598, <https://doi.org/10.1039/C8SE00565F>.
- [28] A.J. Byrd, S. Kumar, L. Kong, H. Ramsurn, R.B. Gupta, Hydrogen production from catalytic gasification of switchgrass biocrude in supercritical water, *Int. J. Hydrogen Energy*. (2011), <https://doi.org/10.1016/j.ijhydene.2010.12.026>.
- [29] Y. Lu, H. Jin, R. Zhang, Evaluation of stability and catalytic activity of Ni catalysts for hydrogen production by biomass gasification in supercritical water, *Carbon Resour. Convers.* (2019), <https://doi.org/10.1016/j.crcon.2019.03.001>.
- [30] H. Su, E. Kanchanapit, D. Wang, H. Zhang, I. Antoni, Z. Mubeen, M.Y. Huang, Catalytic gasification of food waste in supercritical water over La promoted Ni/Al₂O₃ catalysts for enhancing H₂ production, *Int. J. Hydrogen Energy*. 45 (2020) 553–564, <https://doi.org/10.1016/j.ijhydene.2019.10.219>.
- [31] P.W. Dunne, A.S. Munni, C.L. Starkey, T.A. Huddle, E.H. Lester, Continuous-flow hydrothermal synthesis for the production of inorganic nanomaterials, *Philos. Trans. R. Soc. A Math. Phys. Eng. Sci.* 373 (2015) 20150015, <https://doi.org/10.1098/rsta.2015.0015>.
- [32] S. Rodgers, A. Conradie, R. King, S. Poulston, M. Hayes, R. Bommareddy, F. Meng, J. Mckechnie, Reconciling the sustainable manufacturing of commodity chemicals with feasible technoeconomic outcomes, *Johnson Matthey Technol. Rev.* 65 (2021) 375–394, <https://doi.org/10.1595/205651321X16137377305390>.
- [33] E. Lester, M. Gong, A. Thompson, A method for source apportionment in biomass/coal blends using thermogravimetric analysis, *J. Anal. Appl. Pyrolysis*. 80 (2007) 111–117, <https://doi.org/10.1016/j.jaap.2007.01.010>.
- [34] M. Bird, K. Claudia, M. Will, Analysis of biochars for C, H, N, O and S by elemental analyser, in: B. Singh, M. Camps-Arbestain, J. Lehmann (Eds.), *BioChA: A Guide to Analytical Methods*, 1st ed., CRC Press, Australia, 2017, pp. 39–50.
- [35] T. Wu, J.D. Englehardt, A new method for removal of hydrogen peroxide interference in the analysis of chemical oxygen demand, *Environ. Sci. Technol.* 46 (2012) 2291–2298, <https://doi.org/10.1021/es204250k>.
- [36] L. Ferreira-Pinto, A.C. Feirhrmann, M.L. Corazza, N.R.C. Fernandes-Machado, J. S. dos Reis Coimbra, M.D.A. Saldaña, L. Cardozo-Filho, Hydrogen production and TOC reduction from gasification of lactose by supercritical water, *Int. J. Hydrogen Energy*. 40 (2015) 12162–12168, <https://doi.org/10.1016/j.ijhydene.2015.07.092>.
- [37] G. Lin, D. Xu, Z. Ma, S. Wang, Y. Guo, Effect of oxidation coefficient on products of sewage sludge treatment in supercritical water, *Energy Procedia*. 107 (2017) 357–362, <https://doi.org/10.1016/j.egypro.2016.12.176>.
- [38] S.V.P. Mylapilli, S.N. Reddy, Sub and supercritical water oxidation of pharmaceutical wastewater, *J. Environ. Chem. Eng.* 7 (2019), 103165, <https://doi.org/10.1016/j.jece.2019.103165>.
- [39] S. Seif, O. Tavakoli, S. Fatemi, H. Bahmanyar, Subcritical water gasification of beet-based distillery wastewater for hydrogen production, *J. Supercrit. Fluids*. 104 (2015) 212–220, <https://doi.org/10.1016/j.supflu.2015.06.014>.
- [40] T. Bhaskar, B. Balagurumurthy, R. Singh, M.K. Poddar, Chapter 12 - Thermochemical route for biohydrogen production, in: A. Pandey, S.V. Mohan, J.-S. Chang, P.C. Hallenbeck, C. Larroche (Eds.), *Biohydrogen*, Elsevier, Amsterdam, 2013, pp. 285–316, <https://doi.org/10.1016/B978-0-444-59555-3.00012-X>.
- [41] A. Al-Atta, F. Sher, A. Hazafa, A. Zafar, H.M.N. Iqbal, E. Karahmet, E. Lester, Supercritical water oxidation of phenol and process enhancement with in situ formed Fe₂O₃ nano catalyst, *Environ. Sci. Pollut. Res.* (2021), <https://doi.org/10.1007/s11356-021-16390-0>.
- [42] A. Alshammari, V. Kalevaru, A. Martin, Chapter 1 - Metal nanoparticles as emerging green catalysts, in: M. Larramendy, S. Soloneski (Ed.), *Green nanotechnology - Overview and further prospects*, IntechOpen, Rijeka, 2016: p. 1–33. <https://doi.org/10.5772/63314>.
- [43] C. Cao, Y. Zhang, W. Cao, H. Jin, L. Guo, Z. Huo, Transition metal oxides as catalysts for hydrogen production from supercritical water gasification of glucose, *Catal. Letters*. 147 (2017) 828–836, <https://doi.org/10.1007/s10562-017-2002-z>.
- [44] H. Zhang, F. Chen, J. Zhang, Y. Han, Supercritical water gasification of fuel gas production from waste lignin: the effect mechanism of different oxidized iron-based catalysts, *Int. J. Hydrogen Energy*. 46 (2021) 30288–30299, <https://doi.org/10.1016/j.ijhydene.2021.06.169>.
- [45] J.T. Dahle, Y. Arai, Environmental geochemistry of cerium: applications and toxicology of cerium oxide nanoparticles, *Int. J. Environ. Res. Public Health*. 12 (2015) 1253–1278, <https://doi.org/10.3390/ijerph120201253>.
- [46] C.J. Dedman, M.M.I. Rizk, J.A. Christie-Oleza, G.-L. Davies, Investigating the impact of cerium oxide nanoparticles under the ecologically significant marine Cyanobacterium *Prochlorococcus*, *Front. Mar. Sci.* 8 (2021). <https://www.frontiersin.org/article/10.3389/fmars.2021.668097>.
- [47] D. Krewski, R.A. Yokel, E. Nieboer, D. Borchelt, J. Cohen, J. Harry, S. Kacew, J. Lindsay, A.M. Mahfouz, V. Rondeau, Human health risk assessment for aluminium, aluminium oxide, and aluminium hydroxide, *J. Toxicol. Environ. Health. B. Crit. Rev.* 10 (Suppl 1) (2007) 1–269, <https://doi.org/10.1080/10937400701597766>.
- [48] X. Zhu, S. Tian, Z. Cai, Toxicity assessment of iron oxide nanoparticles in zebrafish (*Danio rerio*) early life stages, *PLoS One*. 7 (2012) e46286–e, <https://doi.org/10.1371/journal.pone.0046286>.
- [49] A. Garcia, R. Espinosa, L. Delgado, E. Casals, E. González, V. Puentes, C. Barata, X. Font, A. Sánchez, Acute toxicity of cerium oxide, titanium oxide and iron oxide nanoparticles using standardized tests, *Desalination*. 269 (2011) 136–141, <https://doi.org/10.1016/j.desal.2010.10.052>.
- [50] A.S. Remya, M. Ramesh, M. Saravanan, R.K. Poopal, S. Bharathi, D. Nataraj, Iron oxide nanoparticles to an Indian major carp, *Labeo rohita*: Impacts on hematology, iono regulation and gill Na⁺/K⁺ ATPase activity, *J. King Saud Univ. - Sci.* 27 (2015) 151–160, <https://doi.org/10.1016/j.jksus.2014.11.002>.
- [51] A. Scarso, G. Strukul, Chapter 6 - Catalytic oxidation processes, in: J. Reedijk, K. Poeppelmeier (Eds.), *Comprehensive Inorganic Chemistry II*, 2nd ed., Elsevier, Amsterdam, 2013, pp. 177–221, <https://doi.org/10.1016/B978-0-08-097774-4.00609-4>.
- [52] X. Huang, X. Hou, J. Zhao, L. Zhang, Hematite facet confined ferrous ions as high efficient Fenton catalysts to degrade organic contaminants by lowering H₂O₂ decomposition energetic span, *Appl. Catal. B Environ.* 181 (2016) 127–137, <https://doi.org/10.1016/j.apcatb.2015.06.061>.
- [53] V. Arantes, J. Jellison, B. Goodell, Peculiarities of brown-rot fungi and biochemical Fenton reaction with regard to their potential as a model for bioprocessing biomass, *Appl. Microbiol. Biotechnol.* 94 (2012) 323–338, <https://doi.org/10.1007/s00253-012-3954-y>.
- [54] L.M. Pisarenko, V.I. Lesin, O.T. Kasaikina, Oxidative treatment of biomass using catalysts based on iron(III) oxides, *Russ. Chem. Bull.* 63 (2014) 688–692, <https://doi.org/10.1007/s11172-014-0492-z>.
- [55] F.V.F. Araujo, L. Yokoyama, L.A.C. Teixeira, J.C. Campos, Heterogeneous fenton process using the mineral hematite for the discoloration of a reactive dye solution, *Brazilian J. Chem. Eng.* 28 (2011) 605–616.
- [56] D. Spreitzer, J. Schenk, Reduction of iron oxides with hydrogen—a review, *Steel Res. Int.* 90 (2019) 1900108, <https://doi.org/10.1002/srin.201900108>.
- [57] L. Qian, S. Wang, D. Xu, Y. Guo, X. Tang, L. Wang, Treatment of municipal sewage sludge in supercritical water: a review, *Water Res.* 89 (2016) 118–131, <https://doi.org/10.1016/j.watres.2015.11.047>.
- [58] T. Güngören Madenoğlu, N. Boukis, M. Sağlam, M. Yüksel, Supercritical water gasification of real biomass feedstocks in continuous flow system, *Int. J. Hydrogen Energy*. (2011), <https://doi.org/10.1016/j.ijhydene.2011.08.047>.
- [59] S. Nanda, J. Isen, A.K. Dalai, J.A. Kozinski, Gasification of fruit wastes and agro-food residues in supercritical water, *Energy Convers. Manag.* 110 (2016) 296–306, <https://doi.org/10.1016/j.enconman.2015.11.060>.
- [60] G.A. Naikoo, F. Arshad, I.U. Hassan, M.A. Tabook, M.Z. Pedram, M. Mustaqeem, H. Tabassum, W. Ahmed, M. Rezakazemi, Thermocatalytic hydrogen production through decomposition of methane—a review, *Front. Chem.* 9 (2021), 736801, <https://doi.org/10.3389/fchem.2021.736801>.